Determination of the damping ratio by multi-channel spectral analysis of seismic downhole data

U. Koedel [a,1] and L. Karl [b]

[a] *Helmholtz Centre for Environmental Research - UFZ, Permoserstraße 15, 04318 Leipzig, Germany; uta.koedel@ufz.de*

[b] *Geotomographie GmbH, Am Tonnenberg 18, 56567 Neuwied, Germany; lkarl@geotomographie.de*

Declarations of interest: none.

[1] Corresponding author.

Abstract

Soil dynamic parameters such as shear wave velocity and damping ratio are of major interest in earthquake engineering. While the shear wave velocity, directly linked to the shear modulus, can be determined by a number of laboratory and in-situ tests with satisfying accuracy the damping ratio is much more difficult to obtain. Especially the results of in-situ experiments show often large variations. This is in general due to the troublesome determination of precise signal amplitudes whether in time or frequency domain related with these techniques.

The paper presented comes back to a relationship between attenuation and velocity dispersion of body waves which replaces the measurement of the amplitude characteristics of seismic signals by a frequency dependent velocity function. The implementation of this method has previously shown to be difficult because of the very small levels of dispersion observed in seismic data. Our approach aims to overcome the problem by applying a multi-channel spectral analysis which is widely used in surface wave testing to calculate a velocity dispersion. Multi-channel measurements have shown to be more tolerant to erroneous phase characteristics of single seismic traces than the more common two station measurements.

The velocity dispersion curve is extracted from a phase velocity - frequency spectrum and the damping ratio is calculated by fitting a theoretical dispersion curve to the extracted curve. The method is demonstrated on correlated data of a seismic downhole test performed using a S-wave vibrator source. The obtained results show a reasonable agreement with damping ratios found in

the literature for similar soils.

Key words:
material damping ratio, attenuation, dispersion curve, phase velocity, shear wave.

1 Introduction

The knowledge of dynamic soil parameters is essential to predict the response of soils to dynamic loading and therefore highly relevant in earthquake engineering. Besides the field of earthquake engineering the modeling of seismic wave propagation in order to evaluate the vibrational effects of infrastructural projects on existing buildings and environment is of major concern.

One of the dynamic soil parameters dominating the wave propagation is damping. The damping describes the process of inelastic energy loss of a seismic wave traveling though a medium leading to the attenuation of the amplitude of this wave. The mechanisms causing energy loss are manifold. There are friction attenuation by relative sliding among grains and cracks [1], wave induced fluid flow as squirt-flow [2] and wave induced gas exsolution and dissolution [3] which all convert the elastic wave energy into heat. Another group of mechanisms is wave scattering by heterogeneities such as cracks and pore structures which is influenced by the size, shape and density of the pore fabric and pore-fluid interactions [4]. However, the governing damping mechanisms in soils are not understood thoroughly to allow a sufficient modeling and are summarized in a parameter called material damping ratio D. The material damping ratio represents the inelastic energy dissipation and needs to be distinguished from damping caused by the geometrical spreading of waves.

At small strain levels the material damping is related to the frequency-independent hysteretic damping which appears as hysteresis loop in the stress-strain diagram

[5]. The energy dissipated in the material during one cycle of a harmonic oscillation can be calculated by the inside area of this hysteresis loop. Laboratory tests such as low frequency torsional shear or cyclic triaxial tests make use of the stress-strain behavior and determine the damping ratio directly from the hysteresis loop [6, 7, 8]. Knopoff [9] gives the relationship between the dissipation factor Q^{-1} and a frequency independent damping ratio D:

$$\frac{1}{Q} = \frac{1}{2\pi}\frac{\Delta E}{E} = 2D \tag{1}$$

where ΔE is the energy loss during one loading cycle, E is the peak strain energy stored during the cycle and Q the so called quality factor.

The damping ratio can vary for the different types of body waves in principle. However, the damping ratio estimated from shear waves D_S is considered as the primary quantity of interest in geotechnical engineering [10]. Even though damping is originated from pore-scale mechanisms the soil state on a macro-scale influences the damping ratio. Damping is e.g. sensitive to mean effective stress, void ratio, geological age, cementation, overconsolidation ratio (OCR), plasticity index, cyclic strain, strain rate and the number of loading cycles [11].

In practice, several testing techniques are available to access the small-strain stiffness and also the damping ratio. Among the laboratory measurements the resonant column, torsional shear and the cyclic triaxial test are best established [12]. They are based on observing the behavior of a soil sample at resonance, during free oscillation or making directly use of the measured phase shift between stress and strain. Another approach to obtain small-strain stiffness parameters on the laboratory scale is to measure wave velocities in samples by mean of piezoceramic elements such as bender elements, compressional elements or shear plates [13]. The methods based on piezoceramic elements, especially bender elements, have gained an increasing popularity during the last decades. Occasionally, these methods where extended for the determination of the damping ratio using a spectral ratio [14] or a resonant approach [15, 16]. Although the results of the methods show reasonable agreement regarding the small-strain stiffness, the measured damping ratio often shows major variations. Comparative studies of Cavallaro et al. [17] for instance concluded that damping values obtained from the resonant column test are consistently overestimated in respect to those measured in torsional shear tests.

Nevertheless, laboratory experiments offer the possibility to investigate individual processes and factors influencing the damping ratio closely. They are often essential in the interpretation of in-situ measurements [18, 19, 20, 21]. For example, numerous studies have revealed the importance of the degree of saturation on shear modulus and damping ratio in geomaterials and reported a higher shear modulus and lower damping in unsaturated soils due to the presence of inter-particle suction stresses that increase the soil stiffness [22, 23, 24, 25]. Anyhow, in view of specimen disturbances during soil sampling in-situ measurements have advantages compared to laboratory measurements as they allow the determination of the low strain damping ratio in undisturbed soil [8]. Steward [26] reported for instance that in-situ tests on small strain levels generally give greater damping values compared to those obtained from laboratory tests.

The available in-situ methods divide into crosshole, downhole and surface wave techniques. The crosshole approach focuses in general on the interpretation of horizontally traveling waves. In case of crosshole tomography also inclined wave paths are considered. The borehole based downhole method, also known as Vertical Seismic Profiling (VSP), finds its counterparts in the world of direct-push testing in the shape of Seismic Cone Penetration Test (SCPT) and Seismic Dilatometer Testing (SDMT). Surface wave methods differ in the way of data acquisition either by two receivers only (Spectral Analysis of Surface Waves - SASW) or by a receiver array

(Multichannel Analysis of Surface Waves - MASW) and the kind of data processing. The soil dynamic moduli are regularly calculated based on measured in-situ wave velocities. However, the determination of the damping ratio cannot be considered as an established field technique. Some studies use the half-power bandwidth method for SASW [12], a spectral ratio approach for SCPT and VSP [10, 27, 26], a frequency - wavenumber amplitude regression [28] and an adaption of a theoretical to an experimental mobility function [29] to calculate damping ratio from experimental data. Occasionally the damping ratio is derived from the dispersion properties of seismic waves [10]. In the field of surface wave testing Lai and Rix [30] developed a technique for the simultaneous inversion of surface wave dispersion and attenuation curves taking the coupling between both properties into account. Anyway, Lai and Özcebe [31] reported that D_s and the shear wave velocity V_s are usually still measured independently using different procedures and interpretation methods and therefore neglecting the coupling effect between the two.

Meza-Fajardo and Lai [32, 33] proposed a model of energy dissipation in soils based on a linear viscoelastic material behavior. A distinctive feature of this linear viscoelasticity theory is that the parameters phase velocity $V_\chi(\omega)$, the attenuation coefficient $\alpha_\chi(\omega)$ and $D_\chi(\omega)$ are functions of frequency f, represented by the circular frequency $\omega = 2\pi f$. The index χ denotes for P- or S-wave. The principle of physical causality is satisfied if velocity and damping are not considered independently. Their functional dependency is expressed by the Kramers-Kronig (KK) relation also known as dispersion equations. Meza-Fajardo [32] provided a solution for P-and S-wave phase velocity as a function of the damping ratio. Equation (2) gives the solution for S-waves:

$$\frac{V_S(\omega)}{V_S(0)} = \sqrt{\frac{2\sqrt{1+4D_S^2(\omega)}}{1+\sqrt{1+4D_S^2(\omega)}}} \quad \exp\left[\frac{1}{\pi}\int_{x=0}^{\infty}\frac{\omega^2\arctan\left(2D_S(x)\right)}{x(\omega^2-x^2)}\mathrm{d}x\right] \tag{2}$$

Equation (3) represents the inverse solution for the material damping ratio as a function of the phase velocity:

$$D_S(\omega) = \frac{\frac{2\omega V_S(\omega)}{\pi}\int_{x=0}^{\infty}\frac{\mathrm{d}x}{V_S(x)\,(x^2-\omega^2)}}{\left[\frac{2\omega V_S(\omega)}{\pi}\int_{x=0}^{\infty}\frac{\mathrm{d}x}{V_S(x)\,(x^2-\omega^2)}\right]^2 - 1} \tag{3}$$

where $V_S(0)$ describes the limit of V_S as ω approaches zero. The integrals are of the Cauchy type since they contain a singularity within the integration range for $x = \omega$ which requires special attention while performing the numerical integration.

The dependency between $V_s(\omega)$ and $D_s(\omega)$ stated by the KK relation allows the calculation of one of the two parameters by measurement of the other. Determining the damping ratio reduces therefore to the determination of the dispersion behavior which avoids problems related to measuring accurate signal amplitudes and the compensation of coupling effects of source and receivers required by other techniques.

The solution presented by Meza-Fajardo and Lai [33] is in agreement with a rate-independent damping, i.e. a hysteretic damping, which is often postulated in seismology. Within their paper they showed that there is an excellent agreement of the exact solution of equation (3) to a dispersion relation presented by Liu et al. [34] and later by Aki and Richards [35] which is often used in seismology:

$$V_S(\omega) = \frac{V_S(\omega_{ref})}{1 + \frac{2D_S}{\pi}\ln\frac{\omega_{ref}}{\omega}} \tag{4}$$

Lai and Özcebe [31] determined the damping ratio using equation (2) and (3) for an in-situ crosshole data set. They found that the experimental frequency range of the data was too limited and needed to be extended further to allow more reliable calculations.

Within our paper we present a technique to determine the damping ratio by a multi-channel spectral analysis of seismic downhole data. A shear wave vibrator source was used to generate seismic signals at the surface. Data were acquired by a digital borehole geophone clamped mechanically to the borehole wall. Data gathered in the time domain were transferred into the phase velocity - frequency domain by applying a discrete Fourier transform on the time axis and a discrete slant stack on the distance axis. The phase velocity - frequency spectra of the data was calculated and a dispersion curve was obtained by picking the maximum energy within a certain frequency range. Finally, a numerical fit of the theoretical dispersion relation given in equation (4) to the experimental dispersion curve was carried out to calculate the damping ratio D_S. In our paper we discuss the theoretical background of the dispersion relation used and the determination of the phase velocity - frequency spectra. Furthermore, the experimental results of the downhole study at one test site down to 100 m are presented. Results are compared to available damping values reported in the literature.

2 Theoretical considerations

2.1 Dispersion relation

Aki and Richards [35] showed that any attenuation-dispersion relationship based on causality and considering the definition of the seismic quality factor $Q_S = \omega/[2\alpha_S\,V_S(\omega)]$ must satisfy the following equation:

$$\begin{aligned}\frac{\omega}{V_S(\omega)} &= \frac{\omega}{V_S(\infty)} + \mathrm{H}\left[\alpha_S(\omega)\right] \\ &= \frac{\omega}{\omega(\infty)} + \frac{1}{\pi}\int_{-\infty}^{\infty}\frac{\alpha_S(\omega')}{\omega-\omega'}\mathrm{d}\omega' = 2Q_S\,\alpha_S(\omega) \qquad (5)\end{aligned}$$

where $V_S(\infty)$ is the limit of $V_S(\omega)$ if ω approaches infinity. The Hilbert transform

$\mathrm{H}\left[\alpha_S(\omega)\right]$ returns the function $\alpha_S(\omega)$ with a $\pi/2$ phase shift. If one assumes a constant Q_S equation (5) implies that one has to allow that the phase velocity can vary with frequency to a certain extend. The concept of a constant Q_S is based on the superposition of different relaxation mechanism in soils as described by Liu et al. [34] and Toverud and Ursin [36, 37]. Azimi et al. [38] studied the frequency dependency of the phase velocity. They discussed several absorption models which explain the wave propagation behavior in media. Azimi's second model has been found to agree with many seismic observations and its form of $\alpha_S(\omega)$ has become widely accepted [39]:

$$\alpha_S(\omega) = \frac{\alpha_{S,0}\,\omega}{1+\alpha_{S,1}\,\omega} \tag{6}$$

where $\alpha_{S,0}$ and $\alpha_{S,1}$ are constants and $\alpha_{S,1}\,\omega \ll 1$. With equation (6) the Hilbert transform can be expressed as:

$$\mathrm{H}\left[\alpha_S(\omega)\right] = \frac{2\alpha_{S,0}\,\omega}{\pi(1-\alpha_{S,1}^2\,\omega^2)}\;\ln\frac{1}{\alpha_{S,1}\,\omega} \tag{7}$$

Assuming that the term $\alpha_{S,1}^2\,\omega^2$ can be neglected for $\alpha_{S,1}\,\omega \ll 1$ and large ω one can apply equation (7) to equation (5) and receives:

$$\frac{1}{V_S(\omega)} = \frac{1}{V_S(\infty)} + \frac{2\alpha_{S,0}}{\pi}\;\ln\frac{1}{\alpha_{S,1}\,\omega} \tag{8}$$

Considering the ratio of the phase velocities at two different frequencies ω and ω_{ref} and with $Q^{-1} = 2\alpha_{S,0}\,V_S(\infty) = 2D_S$ one obtains the following dispersion relation:

$$\begin{aligned}\frac{V_S(\omega_{ref})}{V_S(\omega)} &= 1+\frac{2\alpha_{S,0}\,V_S(\infty)}{\pi}\;\ln\frac{\omega_{ref}}{\omega}\\ &\approx 1+\frac{1}{\pi Q_S}\;\ln\frac{\omega_{ref}}{\omega} = 1+\frac{2D_S}{\pi}\;\ln\frac{\omega_{ref}}{\omega}\end{aligned} \tag{9}$$

The equation above (9) is equivalent to equation (4). As stated in the introduction already equation (4) provides a close approximation for the more complex approach given in equation (2) for the case of a constant damping ratio within the frequency range of interest.

Figure 1 illustrates the frequency dependency of the phase velocity given by equation (9) for three constant damping ratios. The figure shows the asymptotic increase of $V_S(\omega)$ with frequency. Greater damping leads to a greater phase velocity increase. The slope of the dispersion curves around the reference frequency is almost proportional to the change of the damping ratio. Therefore, uncertainties in determining the phase velocity will be more significant to smaller damping ratios. In general, phase velocities have to be determined with high accuracy.

[Figure 1 about here.]

2.2 Phase velocity - frequency spectra

In order to be able to make use of the discussed relationship between the phase velocity of the shear wave and the damping ratio, seismic signals at a number of distances from the source have to be recorded. Supposing a repeatable source the signals do not need to originate from the same source event but may be assembled from different events. In any case a data set combining signals recorded at different locations is required. The spacing between the receiver positions and the total length of the receiver array needs to be chosen according to the general rules to avoid spatial aliasing and to ensure a sufficient coverage for long wave lengths.

The dispersion curve, containing the dependency of the phase velocity from the frequency, is obtained by calculating a phase velocity - frequency spectrum from the multi-channel data set. The transfer from the time-distance domain (t, x) into the phase velocity - frequency domain (V, ω) is performed by means of a combination of

Fourier and slant stack transformation. The procedure is comparable to the method of data processing for MASW data described in Park et al. [40].

All wave field transformation techniques to obtain the phase velocity dispersion are based on the assumption that the investigated wave field does not include wave components which velocity depends on the position of the receivers along the covered travel path. If such components are present the method would provide in the best case an averaged dispersion curve. In other cases, e.g. if wavelets are traveling backwards caused by back scattering at embedded objects, voids, fissures or layer interfaces, the generated phase velocity - frequency spectrum is possibly vigorously disturbed and not evaluable at all. Therefore, the path on which the wave transform is to be applied should be carefully selected to avoid inhomogeneous inclusions and abrupt changes of the material stiffness. However, gradual changes of the stiffness, e.g. caused by an increasing overburden pressure, are unavoidable in case of the processing of downhole data. These are covered to certain degree by the averaging behavior of the transformation method.

At first a Fourier transformation is applied to the time-distance representation $u(x,t)$ of the multi-channel data set resulting in the frequency representation $U(x,\omega)$:

$$U(x,\omega) = \int u(x,t)\, \mathrm{e}^{\mathrm{i}\omega t}\, \mathrm{d}t \tag{10}$$

which can be expressed in discrete form as:

$$U(x,\omega) = \sum_{k=1}^{n-1} u(x,t_k)\, \mathrm{e}^{\mathrm{i}\omega t_k}\, (t_{k+1} - t_k) \tag{11}$$

Afterwards the slant stack operation is used on $U(x,\omega)$ with phase velocity V:

$$I(\omega,V) = \int \mathrm{e}^{-\mathrm{i}\frac{\omega}{V}x}\, \frac{U(x,\omega)}{|U(x,\omega)|}\, \mathrm{d}x \tag{12}$$

The effect of geometrical spreading along the receiver layout is compensated by normalizing $U(x,\omega)$ by the amplitudes of its Fourier coefficients $|U(x,\omega)|$. Peaks in the $I(\omega,V)$ field will give the indication for the dispersion curve which can be constructed by following the locus of these peaks along the frequency axis ω.

The representation of equation 12 for discrete arrays is:

$$I(\omega,V)=\sum_{k=1}^{n-1}\mathrm{e}^{-\mathrm{i}\frac{\omega}{V}x_k}\;\frac{U(x_k,\omega)}{|U(x_k,\omega)|}\;(x_{k+1}-x_k) \tag{13}$$

This expression shows that the succession of observation points $(x_{k+1}-x_k)$ does not need to be necessarily equidistant. We will make use of this finding later applying the transformation to non-uniformly spaced experimental data.

3 Field experiment

3.1 Test site

The test site is located in the city of Hannover, Lower Saxony, Germany. Boreholes drilled to a depth of about 100 m are available at the site. Borehole information of one of the boreholes show a lithologic classification into three distinct layers: a shallow layer of quaternary fine and coarse sands down to 6 m, an intermediate layer of quaternary gravel between depths of 6 and 19 m and a cretaceous chalky claystone down to the final depth of the boreholes. A description of the site can be found in Ehosioke [41, 42]. However, previous seismic tomographic results point to a heterogeneity in the subsurface between these two boreholes. A downhole test was carried out at a borehole in about 100 m distance from the borehole from which the site stratigraphy is concluded. The gathered data of this test were used to study the seismic S-wave velocity dispersion behavior in the frequency range up to 100 Hz.

The results are given and discussed within this work.

3.2 Experimental setup

The downhole test was carried out in borehole PRAKLA 1 located at the North-East corner of the site. A sketch of the test set-up can be found in figure 2. The borehole is PVC cased with an inner diameter of 105 mm. A digital three component borehole geophone type BGK1000 was used to acquire P- and S-waves at different depths. The borehole geophone was mechanically clamped to the borehole wall with a defined coupling force to ensure an equal clamping pressure at each depth. The borehole geophone is equipped with a triaxial sensor system consisting of elements of the type GEO OMNI 25-2400 HT. The sensors have a natural frequency of 15 Hz. An in-built magnetic compass was used to obtain the sensor orientation in the borehole.

A S-wave vibrator system MHV-4S developed by Leibnitz Institute of Applied Geoscience (LIAG) with a mass of 4 t and a maximum peak force of 30 kN was used to generate seismic signals with two different excitation direction. The vibrator source produces strong horizontally polarized S-waves. The P-wave component is still sufficient for the identification of the arrival time but its amplitudes are in comparison to the amplitude of the S-wave almost neglectable. Therefore, the application of a window to the signals in order to mute the P-wave can be avoided. Another advantage of using a vibrator system compared to an impact source is to have control on the frequency content of the seismic signals transmitted into the ground. The linear 10 s sweeps were generated within a total recording time of 12 s. The sweep signals ranged from 25 to 150 Hz. The vibrator was located at a distance of 5.40 m from the borehole. Sweeps with opposite excitation direction, i.e. with polarity East (E) and West (W), were generated and recorded.

[Figure 2 about here.]

3.3 Data processing

The correlated seismic traces acquired at the different receiver positions were sorted according to their depths. Based on the compass reading the component giving the particle motion parallel to the vibrator excitation direction was calculated by means of the Alford rotation [43] from the two horizontal channels. Since the multi-receiver record is assembled by single-receiver records the repeatability of the source is of significance. The used vibrator system has shown a high repeatability during previous downhole projects were this issue was checked by means of a surface geophone. Arrival times for P- and S-wave were manually picked using the software ReflexW. Figure 3 shows the rotated seismic signals and the arrival times for the East direction. Besides the P- and S-wave arrivals of the direct traveling waves no obvious other arrivals from reflected or refracted waves can be seen. The S-wave arrival times indicate the presence of two major lithologies, i.e. the quaternary sand-gravel deposits down to a depth of about 35 m (zone 1) followed by the clay stone formation (zone 2). This agrees qualitatively with our knowledge of the site but the depth of the bedrock is very different from the borehole information of the reference borehole in 100 m distance. This confirms the high lateral geological variability of the site. Calculated average seismic velocities of the two identified zones are given in the bar diagram of figure 3.

[Figure 3 about here.]

In order to calculate the damping ratios the phase velocity - frequency spectra were generated following the procedure described in section 2.2. Neither a window nor any filter was applied to the seismic traces. However, due to the normalization of the Fourier coefficients as described in equation 12 those parts of the spectra outside the frequency range of the sweep excitation, i.e. below 25 and above 150 Hz, which contain without normalization only very small amounts of energy, are amplified to the same level as the main frequency range. These parts are virtually meaningless and should not be considered for interpretation.

The data set was divided into two sub sets at the depth of the interface between the two lithological zones. Figure 4 shows the phase velocity - frequency spectra for the two zones on example of the polarization direction E. Phase velocity maxima were manually picked within a frequency range of about 25 to 60 Hz. Additionally, the mean phase velocity V_{Mean} of the picked data was calculated for further reference.

The spectra show besides the branches for the main maxima labeled as A two interesting other features. The first phenomenon, the lower branches labeled as B are due spatial aliasing. The spacing of the virtual receiver array limits the resolution of small wavelengths. The energy of wave components with wavelengths below a certain threshold value are not properly represented and appear ordered to these almost linear lower branches. The second feature are branches above the main branch. The most significant of them is are labeled as C. These are due to spectral leakage in the spatial domain. Parts of the energy of the main branch appears as parallel side branches. The effect intensifies with a shorter total length of the virtual receiver array. Therefore it is more pronounced in the spectrum of zone 1. The array of zone 2 is almost double as long as the array of zone 1.

[Figure 4 about here.]

The simplex search method of Lagarias et al. [44] was applied in order to fit equation 4 to the picked experimental dispersion curve. The independent parameters D_S, $V(\omega_{ref})$ and ω_{ref} of the equation required an optimization with three degrees of freedom. During the iterative procedure a total residual was minimized, in this case the sum of squared differences between the phase velocity of experimental and calculated dispersion curve at the picked frequencies. The three-dimensional optimization used the phase velocity and the frequency at the center of the dispersion curve as initial values for $V(\omega_{ref})$ and ω_{ref}, respectively. The starting value for D_S was visually adjusted according to the approximate slope of the experimental dispersion curve. The optimization process was unconstrained and continued until no significant changes of D_S were observed and the sum of squared residuals reached a minimum.

During the processing of the dispersion curves it became obvious that the fit parameters including D_S are extraordinary sensitive to points of the dispersion curve close to the left and right boundaries of the used frequency range. This phenomenon is known from regression analysis where data points which are far from the majority of data points or lacking neighboring points have an outstanding leverage on the regression results. Such leverage points force the fitted model close to the observed value leading to a small residual [45].

Since the data points on the frequency boundaries have special importance for the result they are picked with great care. If necessary the frequency range is reduce to ensure a high reliability of the data at the boundaries. The results of the dispersion curve fits for the two lithological zones are given in table 1 and graphically displayed in the second part of figure 4. The determined damping ratios are about $D_S = 2.5$ % for zone 1 and about $D_S = 6.6$ % for zone 2.

[Table 1 about here.]

4 Discussion

The damping ratios D_S obtained from model fits for zone 1 range from 2.3 % to 2.7 %. The calculated damping ratios for zone 2 are between 6.3 % and 6.9 %. The results determined for both polarization directions vary only slightly for each zone. This indicates that the applied procedure seems to be fairly robust. Anyhow, we have to admit that no further information on damping ratios are available for the site or even in the Hannover area for similar lithologies and the depth range down to 100 m. Thus, we have to rely on a comparison to available data found in literature which are still rare for certain geologies and geotechnical environments.

Table 2 compiles damping ratios from different literature sources for the same or similar material as found at the test site. It can be noticed that the literature reference values show major variation. A comparison of our experimental damping data with those from literature is given in table 3 and shows a good agreement. The obtained damping ratio for the shallow sediments match well with the measurements of Keiji et al. [46] (2.5 %) and the results for the claystone of zone 2 fall into the range of the findings of Lo Presti and Pallarea [47] (3 to 7 %). In addition, the calculated P- and S-wave velocities from our test site are in accordance to those found in the literature for a similar lithology. Reported velocity values range from 100-300 ms^{-1} for S-wave velocities and 300-1800 ms^{-1} for P-wave velocities in case of silt, sand and gravel. Published velocities for claystone are in the range between 420-800 ms^{-1} for S-wave and 1800-2400 ms^{-1} for P-wave [48, 49].

[Table 2 about here.]

[Table 3 about here.]

5 Conclusion

Our paper presents a method to determine the damping ratio through multi-channel spectral analysis of seismic downhole data. We have demonstrated that the damping ratio can be determined by fitting the dispersion relation presented by Aki and Richards [35] to experimental dispersion curves extracted from phase velocity - frequency spectra. Resulting damping ratios agree well with data published in literature.

From our experiments we can conclude that a high data quality and a sufficiently large frequency range is an important criterion for determining reliable and accurate damping ratios. Manual picking of the dispersion curve at the maxima of the phase velocity - frequency spectra is considered as the most sensitive part of the analysis. This is particularly true if work is carried out at materials where small damping values can be expected. Furthermore, investigated layers need to be large enough to be sampled at a sufficient number of depth locations and large enough to cover the longest wave length investigated.

The multi-channel approach is applicable to experiments where seismic records can be acquired at a number of different distances from the source. It may be applied not only to downhole test data as presented but also to SCPT data. The transfer of the method to crosshole set-ups requires, besides of a suitable borehole source, a larger number of boreholes which will limit the applicability due to economical reasons. It should be also worth investigating if similar results can be obtained using small size vibrators or impulsive S-wave sources.

The study of the method on artificial data to investigate the effects of layer boundaries and abrupt stiffness changes in the area of the processed wave field on the velocity dispersion and the resulting damping ratio deservers an elaborate consideration during future research.

Acknowledgments

The presented work has been funded by the Federal Ministry for Economic Affairs and Energy in the frame of the ZIM program (Zentrales Innovationsprogramm Mittelstand). The financial support for the CPTTOMO project (grand ID ZF4318901LT6 & ZF4315801LT6) is gratefully acknowledged. We thank the LIAG for providing the seismic vibrator for this survey.

References

[1] D.D. Jackson and D.L. Anderson. Physical mechanism of seismic wave attenuation. *Reviews of Geophysics and Space Physics*, 8(1):1–63, February 1970. `https://doi.org/10.1029/RG008i001p00001`.

[2] B. Gurevich, D. Makarynska, O.B. de Paula, and M. Pervukhina. A simple model for squirt-flow dispersion and attenuation in fluid-saturated granular rocks. *Geophysics*, 75(6):N109–N120, 2010. `https://doi.org/10.1190/1.3509782`.

[3] N. Tisato, B. Quintal, S. Chapman, Y. Podladchikov, and J.-P. Burg. Bubbles attenuate elastic waves at seismic frequencies: First experimental evidence. *Geophysical Research Letters*, 42:3880–3887, May 2015. `https://doi.org/10.1002/2015GL063538`.

[4] Z. Wang, R. Wang, T. Li, H. Qiu, and F. Wang. Pore-scale modeling of pore structure effects on p-wave scattering attenuation in dry rocks. *PLOS ONE*, 10(5):1–15, 2015. `https://doi.org/10.1371/journal.pone.0126941`.

[5] C.G. Lai and G.J. Rix. Simultaneous inversion of Rayleigh phase velocity and attenuation for near-surface site characterization. Technical Report No. GIT-CEE/GEO-98-2, School of Civil and Environmental Engineering, Georgia Institute of Technology, 1998.

[6] J. Boaga, S. Renzi, R. Deiana, and G. Cassiani. Soil damping influence on seismic ground response: A parametric analysis for weak to moderate ground motion. *Soil Dynamics and Earthquake Engineering*, 79(A):71–79, December 2015. `https://doi.org/10.1016/j.soildyn.2015.09.002`.

[7] C. Cai, H. Zheng, M.S. Khan, and K.C. Hung. Modeling of material damping properties in ANSYS. In *International ANSYS Conference Proceedings*, 2002.

[8] X. Guo, Y.L. Wong, and Y. Yuan. Estimation of damping ratio of soil sites using microtremor. *Earthquake Engineering and Engineering Vibration*, 1(1):45–49, June 2002. `https://doi.org/10.1007/s11803-002-0006-0`.

[9] L. Knopoff. Q. *Reviews of Geophysics*, 2(4):625–660, November 1964. `https://doi.org/10.1029/RG002i004p00625`.

[10] H. Crow, J.A. Hunter, and D. Motazedian. Monofrequency in situ damping measurements in Ottawa area soft soils. *Soil Dynamics and Earthquake Engineering*, 31(12):1669–1677, December 2011. `https://doi.org/10.1016/j.soildyn.2011.07.002`.

[11] R. Dobry and M. Vucetic. Dynamic properties and seismic response of soft clay deposits. In *International Symposium on Geotechnical Engineering of Soft Soils*, volume 2, pages 51–87, Mexico City, 1987.

[12] S.A. Badsar, M. Schevenels, W. Haegeman, and G. Degrande. Determination of the material damping ratio in the soil from SASW tests using the half-power bandwidth method. *Geophysical Journal International*, 182(3):1493–1508, September 2010. `https://doi.org/10.1111/j.1365-246X.2010.04690.x`.

[13] R. Dyvik and C. Madshus. Lab measurements of G_{max} using bender elements. In *Advances in the Art of Testing Soils Under Cylic Conditions*, pages 186–196, New York, 1985. ASCE.

[14] Y.H. Wang, W.M. Yan, and K.F. Lo. Laboratory and in-situ measurement of attenuation in soil. In Viana da Fonseca & Mayne, editor, *2nd Conference on Geotechnical and Geophysical Site Characterization*, pages 1883–1889, Porto,

2004.

[15] D. Brocanelli and V. Rinaldi. Measurement of low-strain material damping and wave velocity with bender elements in the frequency domain. *Canadian Geotechnical Journal*, 35(6):1032–1040, 1998. https://doi.org/10.1139/t98-058.

[16] L. Karl, W. Haegeman, G. Degrande, and D. Dooms. Determination of the material damping ratio with the bender element test. *Journal of Geotechnical and Geoenvironmental Engineering*, 134(12):1743–1756, 2008. https://doi.org/10.1061/(ASCE)1090-0241(2008)134:12(1743).

[17] A. Cavallaro, G. Lanzo, A. Pagliaroli, M. Maugeri, and D.C.F. Lo Presti. A comparative study on shear modulus and damping ratio of cohesive soil from laboratory tests. In H. Di Benedetto, T. Doanh, H. Geoffroy, and C. Sauzéat, editors, *Proceedings of the 3nd International Symposium on Deformation Characteristics of Geomaterials*, pages 257–265, Lyon, September 2003. A.A. Balkema. https://doi.org/10.1201/NOE9058096043.

[18] B.O. Hardin and V.P. Drnevich. Shear modulus and damping in soils: II Design equations and curves. Technical report, University of Kentucky, Lexington, Kentucky, 1972.

[19] H.B. Seed and I.M. Idriss. Influence of soil conditions on ground motion during earthquakes. *Journal of the Soil Mechanics and Foundations Division, ASCE*, 95:99–137, 1969.

[20] H.B. Seed, R.T. Wong, I.M. Idriss, and K. Tokimatsu. Moduli and damping factors for dynamic analyses of cohesionless soils. *Journal of Geotechnical Engineering*, 112(11):1016–1032, November 1986. https://doi.org/10.1061/(ASCE)0733-9410(1986)112:11(1016).

[21] M. Vucetic and R. Dobry. Effect of soil plasticity on cyclic response. *Journal of Geotechnical Engineering*, 117(1):89–107, January 1991. https://doi.org/10.1061/(ASCE)0733-9410(1991)117:1(89).

[22] M. Ghayoomi and J.S. McCartney. Measurement of small-strain shear moduli of partially saturated sand during infiltration in a geotechnical centrifuge. *Geotechnical Testing Journal*, 34(5):503–513, September 2011. https://doi.org/10.1520/GTJ103608.

[23] L.R. Hoyos, L. Laloui, and R. Vassallo. Mechanical testing in unsaturated soils. *Geotechnical and Geological Engineering*, 26(6):675ff., April 2008. https://doi.org/10.1007/s10706-008-9200-9.

[24] A. Khosravi and J.S. McCartney. Resonant column test for unsaturated soils with suction-saturation control. *Geotechnical Testing Journal*, 34(6):730–739, November 2011. https://doi.org/10.1520/GTJ103102.

[25] B.N. Madhusudhan and J. Kumar. Damping of sands for varying saturation. *Journal of Geotechnical and Geoenvironmental Engineering*, 139(9):1625–1630, September 2013. https://doi.org/10.1061/(ASCE)GT.1943-5606.0000895.

[26] W.P. Stewart. *Insitu measurements of dynamic soil properties with emphasis on damping*. PhD thesis, University of British Columbia, Department of Civil Engineering, Vancouver.

[27] L. Karl, W. Haegeman, and G. Degrande. Determination of the material damping ratio and the shear wave velocity with the seismic cone penetration test. *Soil Dynamics and Earthquake Engineering*, 26(12):1111–1126, 2006. https://doi.org/10.1016/j.soildyn.2006.03.001.

[28] C.J.C. Jones, D.J. Thompson, and M. Petyt. A model for ground vibration from railway tunnels. *Proceedings of the Institution of Civil Engineers - Transport*, 153(2):121–129, 2002. https://doi.org/10.1680/tran.2002.153.2.121.

[29] D.P. Connolly, G. Kouroussis, P.K. Woodward, P. Alves Costa, O. Verlinden, and M.C. Forde. Field testing and analysis of high speed rail vibrations. *Soil Dynamics and Earthquake Engineering*, 67:102–118, December 2014. https://doi.org/10.1016/j.soildyn.2014.08.013.

[30] C.G. Lai, G.J. Rix, S. Foti, and V. Roma. Simultaneous measurement and

inversion of surface wave dispersion and attenuation curves. *Soil Dynamics and Earthquake Engineering*, 22(9-12):923–930, October-December 2002. https://doi.org/10.1016/S0267-7261(02)00116-1.

[31] C.G. Lai and A.G. Özcebe. Non-conventional lab and field methods for measuring frequency-dependent low-strain parameters of soil dynamic behavior. *Soil Dynamics and Earthquake Engineering*, 91:72–86, December 2016. https://doi.org/10.1016/j.soildyn.2016.09.007.

[32] K.C. Meza-Fajardo. *Closed-Form Solutions of the Kramers-Kronig Dispersion Relations in linear Dissipative Continua*. PhD thesis, European School for Advanced Studies in Reduction of Seismic Risk - Rose School, 2005.

[33] K.C. Meza-Fajardo and C.G. Lai. Explicit causal relations between material damping ratio and phase velocity from exact solutions of the dispersion equations of linear viscoelasticity. *Geophysical Journal International*, 171(3):1247–1257, December 2007. https://doi.org/10.1111/j.1365-246X.2007.03590.x.

[34] H.-P. Liu, D.L. Anderson, and H. Kanamori. Velocity dispersion due to anelasticity; implications for seismology and mantle composition. *Geophysical Journal of the Royal Astronomical Society*, 47(1):41–58, October 1976. https://doi.org/10.1111/j.1365-246X.1976.tb01261.x.

[35] K. Aki and P.G. Richards. *Quantitative Seismology*. University Science Books, 2nd edition, 2002.

[36] T. Toverud and B. Ursin. Comparison of seismic attenuation models using zero-offset vertical seismic profiling (VSP) data. *Géophysics*, 70(2):F17–F25, March 2005. https://doi.org/10.1190/1.1884827.

[37] B. Ursin and T. Toverud. Comparison of seismic dispersion and attenuation models. *Studia Geophysica et Geodaetica*, 46(2):293–320, April 2002. https://doi.org/10.1023/A:1019810305074.

[38] SH.A. Azimi, A.V. Kalinin, V.V. Kalinin, and B.L. Pivovarov. Impulse and

transient characteristics of media with linear and quadratic absorption laws. *Izvestiya-Physics of the Solid Earth*, 2:88–93, 1968.

[39] B.J. Brennan and D.E. Smylie. Linear viscoelasticity and dispersion in seismic wave propagation. *Reviews of Geophysics*, 19(2):233–246, 1981. https://doi.org/10.1029/RG019i002p00233.

[40] C.B. Park, R.D. Miller, and J. Xia. Imaging dispersion curves of surface waves on multi-channel record. In *SEG Technical Program Expanded Abstracts 1998*, pages 1377–1380. SEG, 1998. https://doi.org/10.1190/1.1820161.

[41] S.I. Ehosioke. Application of cross-hole seismic tomography in characterization of heterogeneous aquifers. Master's thesis, Georg-August-Universität Göttingen, October 2014.

[42] S.I. Ehosioke and T. Fechner. Application of cross-hole seismic tomography in characterization of heterogeneous aquifers. In *Near Surface Geoscience 2014 - 20th European Meeting of Environmental and Engineering Geophysics*. EAGE, September 2014. https://doi.org/10.3997/2214-4609.20142018.

[43] R.M. Alford. Shear data in the presence of azimuthal anisotropy: Dilley, Texas. In *SEG Technical Program Expanded Abstracts 1986*, pages 476–479, 1986. https://doi.org/10.1190/1.1893036.

[44] J.C. Lagarias, J.A. Reeds, M.H. Wright, and P.E. Wright. Convergence properties of the Nelder-Mead Simplex Method in low dimensions. *SIAM Journal of Optimization*, 9:112–147, 1998. https://doi.org/10.1137/S1052623496303470.

[45] B.S. Everitt and A. Skrondal. *The Cambridge Dictionary of Statistics*. Cambridge University Press, fourth edition, 2010.

[46] T. Keiji, S. Toshihiko, and I. Tsuneo. S wave velocity in the ground and the damping factor. *Bulletin of the International Association of Engineering Geology*, 26(1):327–333, December 1982. https://doi.org/10.1007/BF02594237.

[47] D.C.F. Lo Presti and Pallara O. Damping ratio of soils from laboratory and in-

situ tests. In *Proceedings of the 14th international conference on soil mechanics and foundation engineering*, Hamburg, Germany, September 1997.

[48] A. Keçeli. Soil parameters which can be determined with seismic velocities. *Jeofizik*, 16:17–29, 2012.

[49] J.H. Schön. *Handbook of Petroleum Exploration and Production, Physical Properties of Rocks*, volume 8. Elsevier, 1 edition, 2011.

[50] K.M. Rollins, M.D. Evans, N.B. Diehl, and W.D. Daily III. Shear modulus and damping relationships for gravels. *Journal of Geotechnical and Geoenvironmental Engineering*, 124(5):396–405, May 1998. `https://doi.org/10.1061/(ASCE)1090-0241(1998)124:5(396)`.

[51] M. Bayat and A. Ghalandarzadeh. Stiffness degradation and damping ratio of sand-gravel mixtures under saturated state. *International Journal of Civil Engineering*, 16(10):1261–1277, October 2018. `https://doi.org/10.1007/s40999-017-0274-8`.

[52] B.B. Redpath, R.B. Edwards, R.J. Hale, and F.C. Kintzer. Development of field techniques to measure damping values for near surface rocks and soils. Report prepared for NSF Grant No. PFR-7900192, 1982.

[53] J.-F. Qi, M.-T. Luan, Q. Yang, T.-L. Ma, and Y. Yuan. Dynamic shear modulus and damping ratio of saturated clay. *Chinese Journal of Geotechnical Engineering*, 30(4):518–523, April 2008. (in Chinese).

[54] Y.J. Mok, I. Sanchez-Salinero, K.H. Stokoe II, and J.M. Roesset. In situ damping measurement by crosshole seismic method. In *Earthquake Engineering and Soil Dynamics II. ASCE Spec. Conferences*, volume 20, pages 305–320, Park City, Utah, 1988. ASCE.

List of Figures

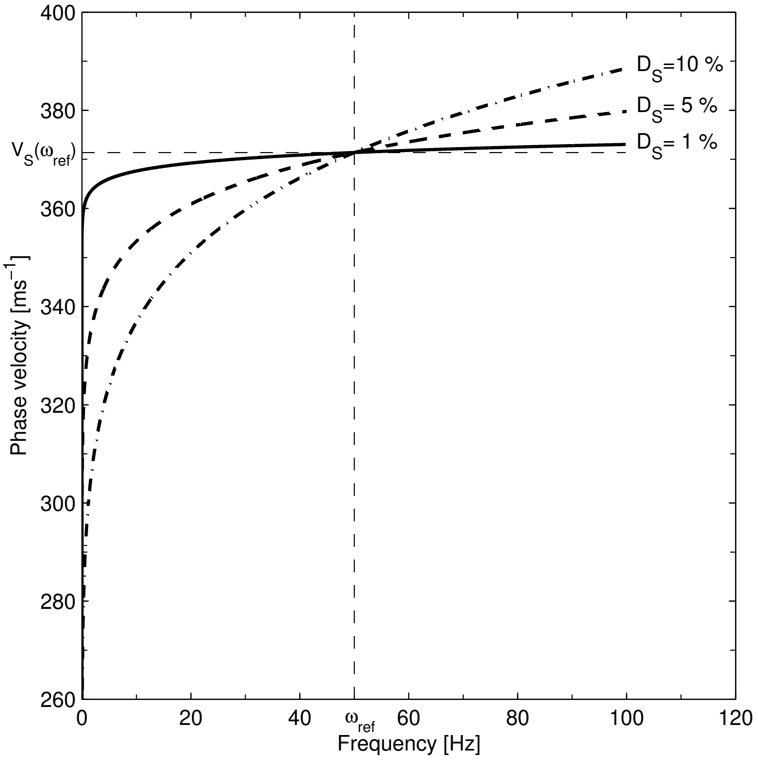

Figure 1. Model data using equation (9) with reference frequency $\omega_{ref} = 2\pi \cdot 50$ s^{-1} and $V_S(\omega_{ref}) = 371.4$ ms^{-1}.

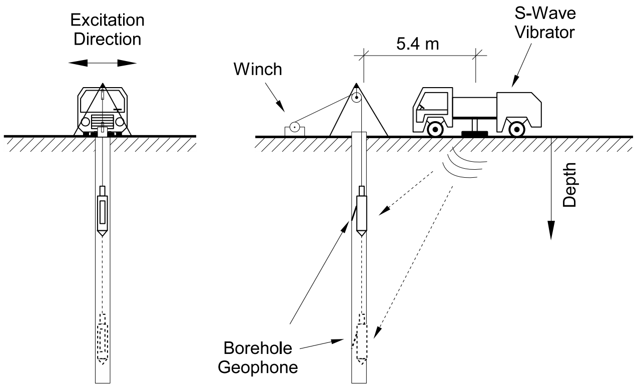

Figure 2. Downhole Test set-up.

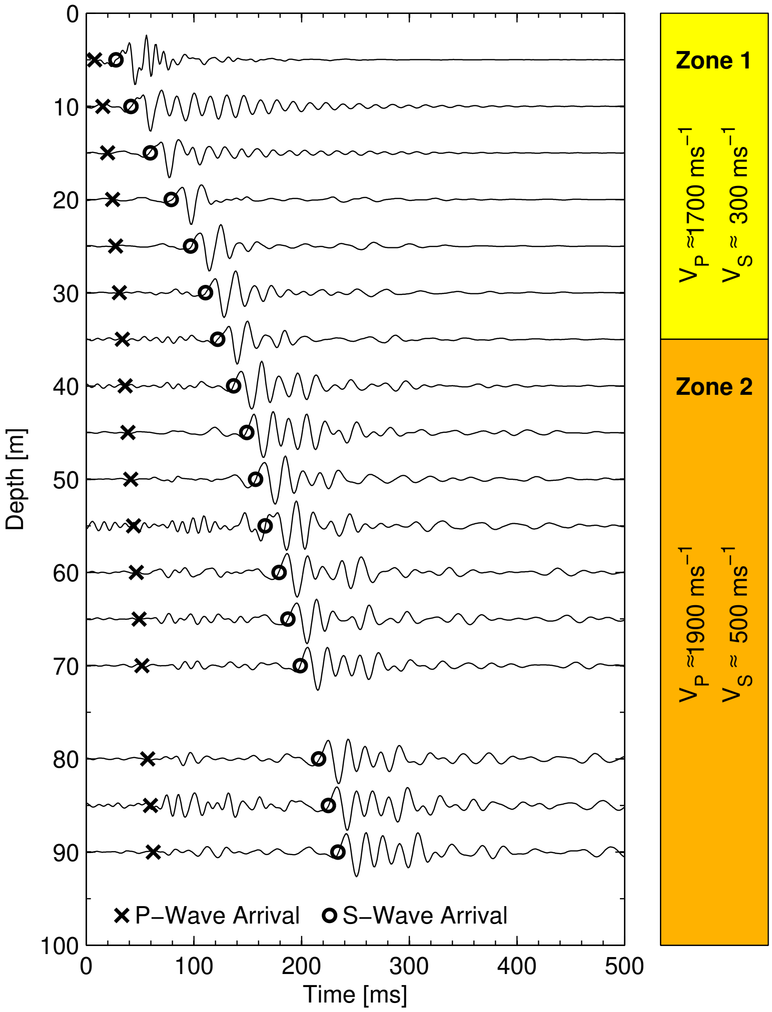

Figure 3. Seismic downhole record rotated in the horizontal plain parallel to vibrator excitation direction E.

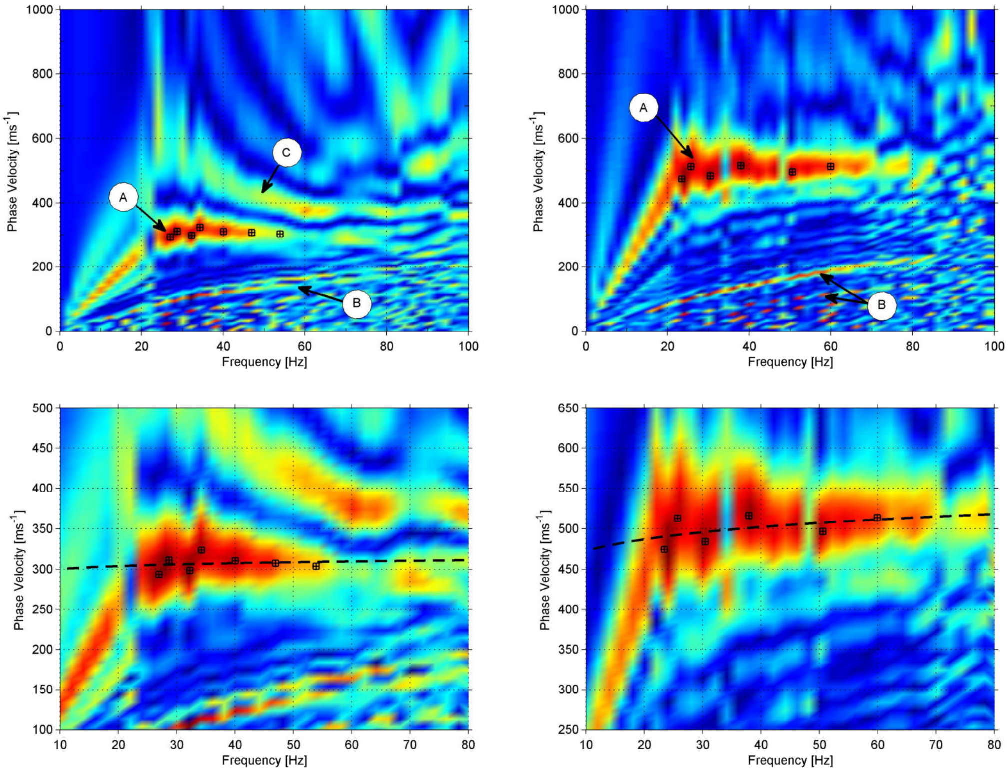

Figure 4. Phase velocity - frequency spectra for excitation direction E; zone 1 (left), zone 2 (right), full view (top), detail view (bottom): extracted dispersion curve points (□), fitted dispersion curve (dashed line), main branches (A), spatial aliasing (B), spectral leakage (C). [should appear in color in print and online]

List of Tables

Table 1
Results of model fit for the two lithological zones and the two excitation directions (E/W).

Zone	Depth	E/W	V_{Mean}	Start Parameters			Fitted Parameters		
				$V(\omega_{ref})$	ω_{ref}	D_S	$V(\omega_{ref})$	ω_{ref}	D_S
	[m]		[ms^{-1}]	[ms^{-1}]	[2π·s^{-1}]	[%]	[ms^{-1}]	[2π·s^{-1}]	[%]
1	5-35	E	306.97	323.85	34.26	3.0	307.00	36.74	2.7
		W	306.90	327.37	34.54	2.0	307.01	37.39	2.3
2	35-90	E	499.67	494.00	42.17	8.0	499.37	35.49	6.9
		W	501.86	484.00	42.17	6.0	501.31	40.64	6.3

Table 2
Reported damping ratio values in literature.

Soil Type	D_S [%]	Reference
Claystone	3-7	Lo Presti & Pallara [47]
Sandstone	1-2	Madhusudhan & Kumar [25]
Gravel (dry)	1-2	Rollins et al. [50]
Saturated sand and clay mixtures	0.05-2	Lo Presti & Pallara [47] Bayat & Ghalandarzadeh [51]
Sandy silt	2.5	Keiji et al. [46]
Sand and clay	1.5-3.5	Redpath et al. [52]
Clay	1.5-2.5 2-5 4-7	Qian et al. [53] Lo Presti & Pallara [47] Mok et al. [54]

Table 3
Characteristic parameters of the assigned zones.

Zone	Depths	Measured Values			Literature References	Lithology
		V_P	V_S	D_S	D_S	
	[m]	[ms^{-1}]	[ms^{-1}]	[%]	[%]	
1	5-35	$\approx$ 1700	$\approx$ 300	2.5	2-3	silt, sand, gravel
2	35-90	$\approx$ 1900	$\approx$ 500	6.6	6-7	claystone